

RESEARCH ARTICLE | MAY 23 2023

A spectral method for the depth-separated solution of a wavenumber integration model for horizontally stratified fluid acoustic waveguides

Tu Houwang (屠厚旺); Wang Yongxian (王勇献) ; Liu Wei (刘巍); ... et. al

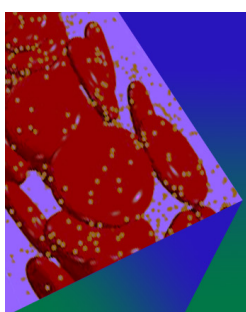


Physics of Fluids 35, 057127 (2023)

<https://doi.org/10.1063/5.0150221>



CrossMark



Physics of Fluids

Special Topic: Flow and Forensics

Submit Today!

 AIP Publishing

A spectral method for the depth-separated solution of a wavenumber integration model for horizontally stratified fluid acoustic waveguides

Cite as: Phys. Fluids **35**, 057127 (2023); doi: [10.1063/5.0150221](https://doi.org/10.1063/5.0150221)

Submitted: 13 March 2023 · Accepted: 2 May 2023 ·

Published Online: 23 May 2023



View Online



Export Citation



CrossMark

Houwang Tu (屠厚旺)^{1,a)} Yongxian Wang (王勇献)^{2,b)} Wei Liu (刘巍)² Shuqing Ma (马树青)² and Xiaodong Wang (王晓东)¹

AFFILIATIONS

¹College of Computer, National University of Defense Technology, Changsha 410073, China

²College of Meteorology and Oceanography, National University of Defense Technology, Changsha 410073, China

^{a)}Electronic mail: tuhouwang@nudt.edu.cn

^{b)}Author to whom correspondence should be addressed: yxwang@nudt.edu.cn

ABSTRACT

The wavenumber integration model is the most precise approach for assessing arbitrary horizontally stratified media within the sphere of computational ocean acoustics. Unlike the normal-mode approach, it considers not only discrete spectra but also continuous spectral components, resulting in fewer model approximation errors for horizontally stratified media. Traditionally, the depth-separated wave equation in the wavenumber integration model has been solved using analytical and semianalytical methods, and numerical solutions have been primarily based on the finite difference and finite element methods. This paper proposes an algorithm for solving the depth equation via the Chebyshev–Tau spectral method, combined with a domain decomposition strategy, resulting in the development of a numerical program named WISpec. The algorithm can simulate the sound field excitation not only from a point source but also from an infinite line source. To that end, the depth equations for each layer are first discretized through the Chebyshev–Tau spectral method and subsequently solved simultaneously by incorporating boundary and interface conditions. Representative numerical experiments are presented to validate the accuracy and speed of WISpec. The high degree of consistency of results obtained from different software tools running the same configuration provides ample evidence that the numerical algorithm described in this paper is accurate, reliable, and numerically stable.

Published under an exclusive license by AIP Publishing. <https://doi.org/10.1063/5.0150221>

I. INTRODUCTION

The wavenumber integration method is among the most established approaches in ocean acoustics. Essentially, an integral transform technique is implemented for horizontally stratified media.¹ Without approximations to the Helmholtz equation, the method completely avoids approximation errors, resulting in a highly accurate method for simulating underwater sound propagation in horizontally stratified media. Comparatively, the normal mode model shares similar mathematical foundations with the wavenumber integration method, differing only in the evaluation strategy for the integral. The normal mode model adopts complex contour integration to reduce the integral to a sum of residues, and the integrals in the wavenumber integration model are evaluated through a numerical quadrature approach.^{2,3} The wavenumber spectrum in a general waveguide comprises both discrete and continuous components. The discrete wavenumber spectrum can be represented by normal modes, while the continuous spectrum must

be described by an integral in the wavenumber domain. In other words, the normal mode model features a limited number of discrete wavenumbers that primarily impact the far field while disregarding the continuous spectrum that may significantly impact the near field, leading to errors. In situations in which the horizontal wavenumbers are near the branch cut, the normal mode model may experience difficulty in finding the roots, hence lowering the accuracy of the numerical sound field. Therefore, the wavenumber integration method is generally considered a precise alternative to the normal mode model.

The concept of wavenumber integration for horizontally stratified media was introduced into ocean acoustics by Pekeris in 1948.⁴ He used simple two- and three-layer structures to model sound propagation in horizontally stratified media. Later, Ewing *et al.* employed this method to study seismic propagation in waveguides with a few layers.⁵ The wavenumber integration technique performs integral transformations on the Helmholtz equation to simplify the original

partial differential equation into a series of ordinary differential equations in depth coordinates. These depth equations are subsequently solved analytically in each layer, and the amplitudes initially remain undetermined. Boundary conditions at the interfaces are then used to calculate the undetermined amplitudes, and the corresponding sound field is ultimately produced by computing the inverse integral transform.

For the initially proposed ocean environment with few layers, the depth equations can easily be solved by expressing the boundary conditions as undetermined sound field amplitudes. However, for more complicated ocean environments, numerical methods are needed, as the undetermined coefficients method is not applicable. The earliest algorithm for simulating depth-dependent wave equations was the propagator matrix approach (PMA), which was proposed by Thomson⁶ and Haskell.⁷ Although the PMA is recursive and requires less memory, a time-consuming correction scheme is required to ensure numerical stability, and it is not well suited for problems that need to be solved at multiple receiver depths.² Kennett reviewed the PMA⁸ and proposed the invariant embedding approach (IEA),⁹ which offers intrinsic numerical stability, recurrence algorithm simplicity, and direct suitability for reflectivity modeling. However, the IEA is not ideal for solving the global problem of interest in ocean acoustics.¹⁰ Currently, the most commonly used method for solving depth equations is the direct global matrix (DGM) approach proposed by Schmidt and Jensen.¹¹ In the DGM approach, the sound field of each layer is expressed as the superposition of the sound field generated by the sound source and an undetermined sound field satisfying the homogeneous depth equation. The continuity conditions at the interfaces control the relationship between the sound fields of each layer. Then, the depth equations of local layers are assembled into a DGM. The sound field in all layers can be obtained simultaneously by solving the global linear equations after imposing the boundary conditions. The main advantage of the DGM approach is its unconditional stability, which means that it yields efficient numerical solutions to the depth-separated wave equations in all layers simultaneously without additional computational costs.¹² The workload and problem size of the DGM are proportional to the number of layers. When acoustic parameters vary greatly with depth or the frequency of the sound source is very high, a denser layer configuration is necessary. In this scenario, the global matrix generated by the DGM approach becomes larger, and the computational speed becomes slower.¹³

In 1988, Schmidt developed a wavenumber integration model called SAFARI, which is based on the DGM approach and can efficiently solve the depth-separated wave equation in fluid/solid horizontally stratified media.¹⁴ In 2022, Schmidt released a new model called OASES, which is an upgraded version of SAFARI that provides improved numerical efficiency. Global matrix mapping has been redefined in OASES to ensure unconditional numerical stability in the few extreme cases in which SAFARI is unstable.¹⁵ Another well-known wavenumber integration model is SCOOTER, which uses the finite element method to discretize the depth-separated wave equation. In SCOOTER, sound pressure and media properties are approximated by piecewise-linear elements, and density is approximated by piecewise constant elements.¹⁶ Additionally, there is a new wavenumber integration normal-mode hybrid model called RPRESS that uses a compound matrix method to solve boundary-value problems.¹⁷

In addition to the widely used finite difference and finite element methods, spectral methods provide an efficient alternative for numerically solving differential equations.¹⁸ Spectral methods offer high accuracy^{19–21} and fast convergence speeds^{22–25} and have been rapidly developed in acoustics,^{26,27} particularly in computational ocean acoustics. Recently, new algorithms using spectral methods have been developed for normal modes,^{28–34} coupled modes,^{35–37} adiabatic modes,³⁸ and parabolic equation models.^{27,39,40} In this article, the Chebyshev–Tau spectral method is used to numerically solve the depth-separated wave equation. The Chebyshev–Tau spectral method does not physically discretize the ocean environment in the vertical direction, avoiding potential errors due to physical discretization using piecewise linear approximation for ocean environmental parameters. The algorithm is also free from any factor that might cause the solution to diverge, making it stable. A corresponding numerical program is developed for this algorithm, and several classic numerical experiments are performed to verify its accuracy and illustrate the capabilities and advantages of the algorithm and scheme designed in this article.

II. MATHEMATICAL MODELING

In horizontally stratified ocean environments, the interfaces at different depths are parallel planes, and the layer properties are solely a function of depth and independent of the azimuthal angle, as illustrated in Fig. 1. For this two-dimensional range-independent problem, the Helmholtz equation is expressed in the following form:²

$$\left[\rho(z) \nabla \cdot \left(\frac{1}{\rho(z)} \nabla \right) + k^2(z) \right] \psi(r, z) = F(r, z), \quad (1)$$

where $\psi(r, z)$ denotes the displacement potential and $F(r, z)$ represents the body force. Here, k defines the wavenumber, $k = 2\pi/c(1 + i\eta\alpha)$, where $\eta = (40\pi \log_{10} e)^{-1}$ and f is the frequency of the source. Additionally, c and α denote the acoustic speed and attenuation of the medium, respectively. The derivations of the sound fields for point and line sources discussed below are based on the Helmholtz equation.

A. Integral transformation for point source problems

Waveguides excited by point sound sources are often explored in cylindrical coordinates. The sound field depends solely on the depth

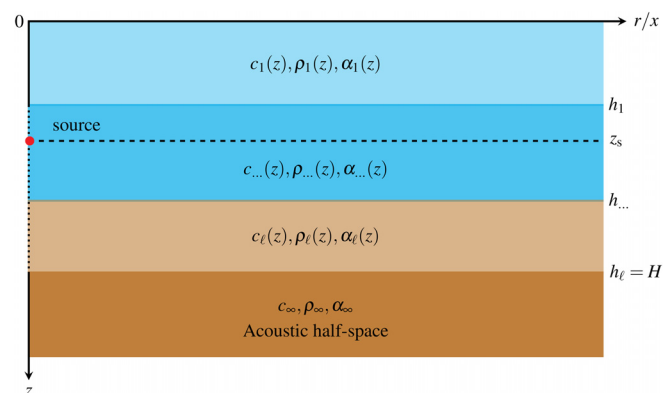


FIG. 1. Schematic of an arbitrary horizontally stratified ocean environment.

and horizontal range from the sound source. To facilitate this approach, we define the z -axis as the vertical axis passing through the sound source and the r -axis parallel to the sea surface, as depicted in Fig. 1. The Helmholtz equation [Eq. (1)] in the cylindrical coordinate system is expressed as follows:

$$\left[\frac{1}{r} \frac{\partial}{\partial r} \left(r \frac{\partial}{\partial r} \right) + \rho(z) \frac{\partial}{\partial z} \left(\frac{1}{\rho(z)} \frac{\partial}{\partial z} \right) + k^2(z) \right] \psi(r, z) = -\frac{\delta(r)\delta(z - z_s)}{2\pi r}, \quad (2)$$

where z_s is the depth of the sound source. We consider using the following Hankel transform pairs for the above equation:

$$\psi(r, z) = \int_0^\infty \Psi(k_r, z) J_0(k_r r) k_r dk_r, \quad (3a)$$

$$\Psi(k_r, z) = \int_0^\infty \psi(r, z) J_0(k_r r) r dr. \quad (3b)$$

Specifically, the following operation is applied to Eq. (2):

$$\int_0^\infty (\cdot) J_0(k_r r) r dr.$$

Therefore, we can easily obtain the following depth-separated wave equation:

$$\left[\rho(z) \frac{d}{dz} \left(\frac{1}{\rho(z)} \frac{d}{dz} \right) + (k^2 - k_r^2) \right] \Psi(k_r, z) = -\frac{\delta(z - z_s)}{2\pi}. \quad (4)$$

This equation is an ordinary differential equation for different depths that can be solved numerically or analytically. Conventionally, the solution strategy for the Green function $\Psi(k_r, z)$ involves first physically discretizing the ocean environment in the depth direction.^{6–8,12} The ocean environment is partitioned into sufficiently thin layers, and the acoustic parameters of each layer are treated as depth-independent constants, introducing errors. In this paper, we propose a Chebyshev–Tau spectral method to numerically solve the depth-separated wave equation; this is a high-precision numerical approach that does not require physical discretization. Once $\Psi(k_r, z)$ has been determined at various discrete wavenumbers for the selected receiver depths, Eq. (3a) can be evaluated to yield the total displacement potential $\psi(r, z)$ at any depth and distance.

B. Integral transformation for line source problems

An infinitely long line sound source is commonly used to verify the accuracy of models in computational ocean acoustics. Here, we also consider the solution of this standard model. Usually, the line source problem is presented in a Cartesian coordinate system. We still define the z -axis to be vertically downward and passing through the sound source. The x -axis is parallel to the sea surface, and the sound source extends into the xoz -plane perpendicular to infinity. The principal structure is depicted in Fig. 1, with the r -axis corresponding to the x -axis in this scenario. Therefore, the Helmholtz equation for the line source in the Cartesian coordinate system is given by,²

$$\left[\frac{\partial^2}{\partial x^2} + \rho(z) \frac{\partial}{\partial z} \left(\frac{1}{\rho(z)} \frac{\partial}{\partial z} \right) + k^2(z) \right] \psi(x, z) = -\delta(x)\delta(z - z_s). \quad (5)$$

We apply the following Fourier transform pairs to Eq. (5):

$$\psi(x, z) = \int_{-\infty}^{\infty} \Psi(k_x, z) e^{ik_x x} dk_x, \quad (6a)$$

$$\Psi(k_x, z) = \frac{1}{2\pi} \int_{-\infty}^{\infty} \psi(x, z) e^{-ik_x x} dx. \quad (6b)$$

Specifically, the following operator is applied to the above formula:

$$\frac{1}{2\pi} \int_{-\infty}^{\infty} (\cdot) e^{-ik_x x} dx.$$

The following depth-separated wave equation is, thus, obtained:

$$\left[\rho(z) \frac{d}{dz} \left(\frac{1}{\rho(z)} \frac{d}{dz} \right) + (k^2 - k_x^2) \right] \Psi(k_x, z) = -\frac{\delta(z - z_s)}{2\pi}. \quad (7)$$

Solving Eq. (7) yields the depth-dependent Green function $\Psi(k_x, z)$. After $\Psi(k_x, z)$ is obtained, the total sound field can be synthesized using Eq. (6a), as discussed for a point source.

A comparison of Eqs. (4) and (7) reveals that the depth-separated wave equations for the point source and line source have identical forms, except that r is replaced with x and k_r is replaced by k_x . Consequently, the Green function of the depth-separated wave equation can be used as the integral kernel function not only for the point source but also for the line source. Here, we present only Eq. (4) as an example of the solution method for the depth-separated wave equation.

C. Interface and boundary conditions

In the ocean environment depicted in Fig. 1, the interfaces ($\{h_l\}_{l=1}^{\ell-1}$) with discontinuous environmental parameters in seawater are constrained by interface conditions. In accordance with the connection between sound pressure and displacement potential, the sound pressure and normal particle velocity are governed by continuity, yielding

$$\rho(h_l^+) \Psi(k_r, h_l^+) = \rho(h_l^-) \Psi(k_r, h_l^-), \quad l = 1, 2, \dots, \ell - 1, \quad (8a)$$

$$\left. \frac{d\Psi}{dz} \right|_{z=h_l^+} = \left. \frac{d\Psi}{dz} \right|_{z=h_l^-}, \quad l = 1, 2, \dots, \ell - 1, \quad (8b)$$

where the superscripts – and + denote the interfaces from above and below, respectively.

The detailed solution to Eq. (4) involves the boundary conditions at the sea surface ($z = 0$) and the seabed ($z = H$). Due to the significant difference in impedance between seawater and air, the sea surface is typically assumed to be perfectly reflected, corresponding to a pressure-release boundary,

$$\psi(r, 0) = 0 \iff \Psi(k_r, 0) = 0. \quad (9)$$

Regarding the lower boundary condition, two common options are a pressure-release seabed and a rigid seabed,

$$\psi(r, H) = 0 \iff \Psi(k_r, H) = 0, \quad (10a)$$

$$\left. \frac{d\psi_\ell(r, z)}{dz} \right|_{z=H} = 0 \iff \left. \frac{d\Psi_\ell(k_r, z)}{dz} \right|_{z=H} = 0. \quad (10b)$$

Moreover, when constructing ocean environment models, the acoustic half-space boundary presented in Fig. 1 is typically utilized. The lower

boundary condition that must be observed on the truncated bottom of the acoustic half-space takes the following form:

$$\rho_\infty \frac{d\Psi_\ell}{dz} \Big|_{z=H} + \rho_\ell(H) \sqrt{k_r^2 - k_\infty^2} \Psi_\ell \Big|_{z=H} = 0. \quad (11)$$

Note that the inhomogeneous term on the right-hand side of Eq. (4) involves the source term $\delta(z - z_s)$, requiring special treatment of the equation at the depth of the sound source. To address this singularity, we introduce an artificial interface at the depth of the sound source.

Because of the singularity at the sound source, we cannot apply the continuity condition Eq. (8b) to constrain the normal particle velocity. Therefore, we naturally aim to integrate both sides of Eq. (4) in an exceedingly small neighborhood v of z_s to eliminate $\delta(z - z_s)$,

$$\int_{z_s-v}^{z_s+v} \left[\rho(z) \frac{d}{dz} \left(\frac{1}{\rho(z)} \frac{d\Psi}{dz} \right) + (k^2 - k_r^2) \Psi \right] dz = -\frac{1}{2\pi}. \quad (12)$$

Since $v \rightarrow 0$, the above equation translates to

$$\frac{d\Psi}{dz} \Big|_{z_s-v}^{z_s+v} = -\frac{1}{2\pi} \iff \frac{d\Psi}{dz} \Big|_{z_s^+} - \frac{d\Psi}{dz} \Big|_{z_s^-} = -\frac{1}{2\pi}. \quad (13)$$

This represents the interface condition that the displacement potential must satisfy at the depth of the sound source.

D. Wavenumber integration

After obtaining the Green function for Eq. (4) or (7), the displacement potential field can be obtained by evaluating the inverse Hankel/Fourier transform. However, in numerical calculations using Eq. (3a) or (6a) to compute the displacement potential field of a point or line source, only a finite interval $[k_{\min}, k_{\max}]$ and M discrete points are utilized for numerical integration. This poses a challenge, as undersampling the spikes in the Green function may introduce significant errors. Moreover, waveguides typically have poles located on or near the real wavenumber axis, exacerbating the aliasing issue. Fortunately, the problem can be resolved by shifting the integral contour into the complex plane, as detailed in Chapter 4.5.5 of Ref. 2. A contour offset ε can be introduced, and by selecting points at which the kernel functions are small and the contour offset satisfies $\varepsilon \ll (k_{\max} - k_{\min})$, the contributions of the vertical components become insignificant relative to the components in the horizontal direction. Substituting $\bar{k} = k_r - i\varepsilon$ into Eqs. (3a) and (6a) yields

$$\psi(r, z) = \int_0^\infty \Psi(k_r - i\varepsilon, z) J_0[(k_r - i\varepsilon)r](k_r - i\varepsilon) dk_r, \quad (14a)$$

$$\begin{aligned} \psi(x, z) &= \int_{-\infty}^\infty \Psi(k_x - i\varepsilon, z) \exp[i(k_x - i\varepsilon)x] dk_x \\ &= 2 \int_0^\infty \Psi(k_x - i\varepsilon, z) \cos[(k_x - i\varepsilon)x] dk_x. \end{aligned} \quad (14b)$$

For most practical purposes, the value of ε can be determined as follows:²

$$\varepsilon = \frac{3\Delta k_r}{2\pi \log_{10} e}, \quad \Delta k_r = \frac{k_{\max} - k_{\min}}{M - 1}. \quad (15)$$

Therefore, the integrals in Eq. (14) become rectangular integrals of the following form in the actual numerical calculations:

$$\psi(r, z) = \Delta k_r \sum_{k_r=k_{\min}}^{k_{\max}} \Psi(k_r - i\varepsilon, z) J_0[(k_r - i\varepsilon)r](k_r - i\varepsilon), \quad (16a)$$

$$\psi(x, z) = 2\Delta k_x \sum_{k_x=k_{\min}}^{k_{\max}} \Psi(k_x - i\varepsilon, z) \cos[(k_x - i\varepsilon)x]. \quad (16b)$$

Δk_x shares the form of Δk_r in Eq. (15). The numerical integration outlined above can be conveniently formulated as matrix multiplication. Furthermore, it is crucial to select the numerical integration parameters carefully, specifically Δr , k_{\min} , k_{\max} , and the farthest range r_{\max} of the sound field under consideration. It is worth noting that popular integral evaluation techniques, such as quadrature schemes and fast field techniques, are widely applicable and not the primary focus of this article; accordingly, they will not be discussed in detail.

When the displacement potential field is obtained with the above numerical integration, the sound pressure field can be obtained with the following formula:⁴¹

$$p(r, z) = \rho(z)\omega^2 \psi(r, z), \quad (17a)$$

$$p(x, z) = \rho(z)\omega^2 \psi(x, z), \quad (17b)$$

where $\omega = 2\pi f$. The transmission loss (TL) is defined as

$$TL = -20 \log_{10} \left| \frac{p}{p_0} \right|, \quad p_0 = \begin{cases} \frac{\rho_s \omega^2}{4\pi} \exp(ik_s), & \text{point source,} \\ \frac{i\rho_s \omega^2}{4} \mathcal{H}_0^{(1)}(k_s), & \text{line source.} \end{cases} \quad (18)$$

Here, p_0 is the acoustic pressure 1 m from the source; ρ_s and k_s are the density and wavenumber of the medium at the location of the source, respectively; and $\mathcal{H}_0^{(1)}(\cdot)$ denotes the first type of Hankel function.

As per the theoretical framework outlined above, the Green function in Eqs. (4) and (7) serves as the cornerstone of the wavenumber integration model. The primary innovation of this paper involves proposing a new algorithm based on the spectral method to yield a numerical solution to the Green function in Eqs. (4) and (7).

III. NUMERICAL DISCRETIZATION

A. Chebyshev–Tau spectral method

Subsequently, we utilize the Chebyshev–Tau spectral method to solve the depth-separated wave equation, i.e., Eq. (4). To that end, Chebyshev polynomials serve as the basis functions in this spectral method,²³ therefore, a brief introduction to these polynomials is warranted,

$$\begin{aligned} T_0(t) &= 1, & T_1(t) &= t, \\ T_{i+1}(t) &= 2tT_i(t) - T_{i-1}(t), & i &\geq 1. \end{aligned} \quad (19)$$

Chebyshev polynomials are a class of orthogonal polynomials with orthogonality defined as follows:²⁵

$$\int_{-1}^1 \frac{T_i(t)T_j(t)}{\sqrt{1-t^2}} dt = \begin{cases} 0, & i \neq j, \\ \pi, & i = j = 0, \\ \frac{\pi}{2}, & i = j \geq 1. \end{cases} \quad (20)$$

Since the Chebyshev polynomials $\{T_i(t)\}$, that is, the basis functions, are defined in $t \in [-1, 1]$, the equation to be solved, Eq. (4), must first be scaled to $t \in [-1, 1]$ as follows:

$$\mathcal{L}\Psi(t) = 0, \quad \mathcal{L} = \frac{4}{|\Delta h|^2} \rho(t) \frac{d}{dt} \left(\frac{1}{\rho(t)} \frac{d}{dt} \right) + [k^2(t) - k_r^2], \quad (21)$$

where Δh denotes the length of the domain and \mathcal{L} is the differential operator.

Next, the function to be determined, $\Psi(t)$, is transformed into the spectral space spanned by the basis functions $\{T_i(t)\}_{i=0}^\infty$. Furthermore, the expression for the spectral coefficients $\{\hat{\Psi}_i\}_{i=0}^\infty$ can also be obtained from the orthogonality of the Chebyshev polynomials²⁴

$$\begin{aligned} \Psi(t) = \sum_{i=0}^{\infty} \hat{\Psi}_i T_i(t) \iff \hat{\Psi}_i = \frac{2}{\pi d_i} \int_{-1}^1 \frac{T_i(t)\Psi(t)}{\sqrt{1-t^2}} dt, \\ d_i = \begin{cases} 2, & i = 0, \\ 1, & i > 0. \end{cases} \end{aligned} \quad (22)$$

The integral on the right side of the above equation is usually calculated using the Gauss–Chebyshev–Lobatto numerical quadrature.²³

Since it is impossible to expand this expression to infinite terms in actual calculations, only the first $(N+1)$ terms can be retained²²

$$\Psi(t) \approx \Psi_N(t) = \sum_{i=0}^N \hat{\Psi}_i T_i(t). \quad (23)$$

The function approximation $\Psi_N(t)$ becomes increasingly precise with increasing N , and the orthogonality between the basis functions ensures rapid convergence of the series truncation errors. Nevertheless, truncating the infinite term expansion, as described above, unavoidably produces errors, thereby causing Eq. (21) to no longer strictly hold. By substituting $\Psi_N(t)$ into Eq. (21), a residual,²⁰ referred to as $R_N(t)$, can be identified,

$$R_N(t) = \mathcal{L}\Psi_N(t). \quad (24)$$

A principle must be adopted to minimize R_N so that the accuracy of the above spectral expansion can be increased. In a Tau-type spectral method, the basis functions are utilized as weight functions, and the inner products of the weight functions and residuals are set to zero⁴²

$$\int_{-1}^1 \frac{\mathcal{L}\Psi_N(t)T_i(t)}{\sqrt{1-t^2}} dt = 0, \quad i = 0, 1, \dots, N. \quad (25)$$

This weighted residual method²⁵ enforces constraints on the residuals. In mathematical texts, the above equation is referred to as the variational form or weak form of Eq. (21).²³ By taking into account the Chebyshev polynomials' orthogonality and Eq. (22), the above equation can be expressed as

$$\widehat{\mathcal{L}}\hat{\Psi}_i = 0, \quad i = 0, 1, \dots, N, \quad (26)$$

where $\widehat{\mathcal{L}}$ represents the \mathcal{L} operator in the spectral space.

The transformation of the \mathcal{L} operator to the spectral space, denoted by $\widehat{\mathcal{L}}$, is a crucial task. The \mathcal{L} operator encompasses a derivative term. Based on the properties of the Chebyshev polynomial, we can demonstrate the following:

$$\widehat{\Psi}'_i = \frac{2}{c_i} \sum_{\substack{j=i+1, \\ j+i=\text{odd}}}^N j \widehat{\Psi}_j, \quad c_0 = 2, c_{i>1} = 1 \iff \widehat{\Psi}' = \mathbf{D}_N \widehat{\Psi}. \quad (27)$$

Consequently, the derivative term is transformed into a differential matrix \mathbf{D}_N , which depends solely on the truncation order N and is entirely independent of Ψ . The relationship between Chebyshev polynomials and their derivatives is used to establish this term.²⁴

The \mathcal{L} operator also encompasses a product term, and the spectral transformation of the product of two functions satisfies the following relationship:

$$(\widehat{v\Psi})_i \approx \frac{1}{2} \sum_{m+n=i}^N \widehat{\Psi}_m \widehat{v}_n + \frac{1}{2} \sum_{|m-n|=i}^N \widehat{\Psi}_m \widehat{v}_n \iff (\widehat{v\Psi}) \approx \mathbf{C}_v \widehat{\Psi}, \quad (28)$$

where $v = v(t)$ refers to any continuous function in $t \in [-1, 1]$, for example. The relationship between the spectral coefficients of the product of two functions and the spectral coefficients of the individual functions is likewise captured by a matrix \mathbf{C}_v . This matrix depends solely on v and not on Ψ .^{19,23}

B. Discretization

According to the above analysis, Eq. (21) is discretized into the following matrix–vector form in the Chebyshev spectral space:

$$\left(\frac{4}{|\Delta h|^2} \mathbf{C}_\rho \mathbf{D}_N \mathbf{C}_{1/\rho} \mathbf{D}_N + \mathbf{C}_{k^2} - k_r^2 \mathbf{E}_N \right) \widehat{\Psi} = \mathbf{0}, \quad (29)$$

where \mathbf{E}_N is the $(N+1)$ -order identity matrix. The above equation is equivalent to Eq. (26), where $\widehat{\Psi}$ is a column vector composed of $\{\widehat{\Psi}_i\}_{i=0}^N$. Equation (29) is a set of linear equations, and the boundary conditions are not imposed at this time.

To establish the depth-separated wave equation for the waveguide depicted in Fig. 1, we need to formulate this equation for all the discontinuous layers. A single set of basis functions cannot span all the layers, as the Chebyshev polynomials fail to meet the continuity conditions at the interfaces $\{h_l\}_{l=1}^\ell$. The Gibbs phenomenon arises when orthogonal basis functions are employed to expand discontinuous functions.⁴³ Therefore, we adopt a domain-decomposition strategy⁴⁴ for Eq. (4) and partition the entire domain into ℓ subintervals

$$\begin{aligned} \Psi_l(z) = \Psi_l(t) &\approx \sum_{i=0}^{N_l} \widehat{\Psi}_{l,i} T_i(t), \\ t &= \frac{2z}{h_{l-1} - h_l} + \frac{h_l + h_{l-1}}{h_l - h_{l-1}}, \quad z \in [h_{l-1}, h_l]. \end{aligned} \quad (30)$$

N_l is the spectral truncation order in the l th layer and $\{\widehat{\Psi}_{l,i}\}_{i=0}^{N_l}$ is the spectral coefficient in the l th layer. Similar to Eq. (29), the depth-separated wave equation for the l th layer can be discretized into the following matrix–vector form:

$$\mathbf{A}_l \hat{\Psi}_l = \mathbf{0}, \quad \mathbf{A}_l = \frac{4}{(h_l - h_{l-1})^2} \mathbf{C}_{\rho_l} \mathbf{D}_{N_l} \mathbf{C}_{1/\rho_l} \mathbf{D}_{N_l} + \mathbf{C}_{k_l^2} - k_r^2 \mathbf{E}_{N_l}, \quad (31)$$

where \mathbf{A}_l is a square matrix of order $(N_l + 1)$ and $\hat{\Psi}_l$ is a column vector composed of $\{\hat{\Psi}_{l,i}\}_{i=0}^{N_l}$. Since the interface conditions are related to the adjacent layers, a total of ℓ Eq. (31) of $l = 1, \dots, \ell$ should be solved simultaneously, which is expressed as follows:

$$\begin{bmatrix} \mathbf{A}_1 & \mathbf{0} & \mathbf{0} & \mathbf{0} \\ \mathbf{0} & \mathbf{A}_2 & \mathbf{0} & \mathbf{0} \\ \mathbf{0} & \mathbf{0} & \ddots & \mathbf{0} \\ \mathbf{0} & \mathbf{0} & \mathbf{0} & \mathbf{A}_\ell \end{bmatrix} \begin{bmatrix} \hat{\Psi}_1 \\ \hat{\Psi}_2 \\ \vdots \\ \hat{\Psi}_\ell \end{bmatrix} = \begin{bmatrix} \mathbf{0} \\ \mathbf{0} \\ \vdots \\ \mathbf{0} \end{bmatrix}. \quad (32)$$

Note that when z_s is not at the interface, we establish a virtual interface, as described in Eq. (13). Equation (32), which is modified to be satisfied for the two layers above and below the virtual interface, can also be organized into block diagonal form, and the total number of layers becomes $(\ell + 1)$ at this time,

$$\begin{bmatrix} \mathbf{A}_1 & \mathbf{0} & \mathbf{0} & \mathbf{0} & \mathbf{0} \\ \mathbf{0} & \ddots & \mathbf{0} & \mathbf{0} & \mathbf{0} \\ \mathbf{0} & \mathbf{0} & \mathbf{A}_s & \mathbf{0} & \mathbf{0} \\ \mathbf{0} & \mathbf{0} & \mathbf{0} & \ddots & \mathbf{0} \\ \mathbf{0} & \mathbf{0} & \mathbf{0} & \mathbf{0} & \mathbf{A}_{\ell+1} \end{bmatrix} \begin{bmatrix} \hat{\Psi}_1 \\ \vdots \\ \hat{\Psi}_s \\ \vdots \\ \hat{\Psi}_{\ell+1} \end{bmatrix} = \begin{bmatrix} \mathbf{0} \\ \vdots \\ \mathbf{0} \\ \vdots \\ \mathbf{0} \end{bmatrix}, \quad (33)$$

where \mathbf{A}_s and $\hat{\Psi}_s$ are as defined in Eq. (31) in the layer at the depth of the sound source.

The interface and boundary conditions presented in Eq. (8) and Eqs. (9)–(11), respectively, must be transformed to the spectral space and explicitly incorporated into Eq. (33). Furthermore, the intermittent condition specified in Eq. (13) must also be added to Eq. (33) at the virtual interface located at the depth of the sound source. Taking into account the virtual interface, the seawater media consists of $(\ell + 1)$ layers, resulting in ℓ interfaces and 2ℓ interface conditions. In addition, the boundary conditions at the sea surface ($z = 0$) and seabed ($z = H$) add $2(\ell + 1)$ more conditions to be applied. Next, we provide a detailed description of how to impose these boundary and interface conditions. For ease of discussion, we introduce the following intermediate row vectors:

$$\mathbf{s}_l = [s_0, s_1, s_2, \dots, s_{N_l}], \quad \mathbf{q}_l = [q_0, q_1, q_2, \dots, q_{N_l}],$$

where $s_i = T_i(-1) = (-1)^i$, $q_i = T_i(+1) = 1$. Thus, the interface conditions and boundary conditions of Eqs. (8)–(11) and (13) can be transformed in Chebyshev spectral space as

$$\rho(h_l^+) \mathbf{s}_l \hat{\Psi}_{l+1} - \rho(h_l^-) \mathbf{q}_l \hat{\Psi}_l = 0, \quad (34a)$$

$$\mathbf{s}_l \mathbf{D}_{N_{l+1}+1} \hat{\Psi}_{l+1} / (h_l - h_{l+1}) - \mathbf{q}_l \mathbf{D}_{N_l+1} \hat{\Psi}_l / (h_{l-1} - h_l) = 0, \quad (34b)$$

$$\mathbf{q}_1 \hat{\Psi}_1 = 0, \quad (34c)$$

$$\mathbf{s}_{\ell+1} \hat{\Psi}_{\ell+1} = 0, \quad (34d)$$

$$(34e)$$

$$\left[2\rho_\infty \mathbf{s}_{\ell+1} \mathbf{D}_{N_{\ell+1}+1} / (h_l - h_{l+1}) + \rho(H) \sqrt{k_r^2 - k_\infty^2} \mathbf{s}_{\ell+1} \right] \hat{\Psi}_{\ell+1} = 0, \quad (34f)$$

$$\mathbf{s}_{s+1} \mathbf{D}_{N_{s+1}+1} \hat{\Psi}_{s+1} / (h_s - z_s) - \mathbf{q}_s \mathbf{D}_{N_s+1} \hat{\Psi}_s / (z_s - h_{s+1}) = -\frac{1}{4\pi}, \quad (34g)$$

where h_s and h_{s+1} represent the depth of the interfaces above and below the sound source, respectively.

How do these $2(\ell + 1)$ conditions apply to Eq. (33)? One approach is to substitute the last two rows of the \mathbf{A}_1 to $\mathbf{A}_{\ell+1}$ block matrix with the corresponding boundary or interface conditions that each layer must satisfy. This procedure reduces the spectral accuracy of each layer from order N_l to order $(N_l - 2)$, but this can be overcome by increasing the value of N_l . By solving Eq. (33) with added boundary constraints, we can obtain the spectral coefficients $\{\hat{\Psi}_l\}_{l=1}^{\ell+1}$ for each layer of the Green function. To determine the numerical solution of $\Psi(k_r, z)$, we perform the inverse Chebyshev transform [Eq. (23)] of the spectral coefficients $\{\hat{\Psi}_l\}_{l=1}^{\ell+1}$ sequentially and combine them into a single column vector.

IV. NUMERICAL SIMULATION

We present a program named WISpec (wavenumber integration based on the spectral method) developed based on the above algorithm and verify the accuracy of the algorithm through several numerical experiments.

A. Analytical example: Ideal fluid waveguide

The ideal fluid waveguide is a very simple example with an analytical solution. It consists of a layer of homogeneous seawater and upper and lower boundaries; the sea surface is usually perfectly free, and the bottom can be perfectly free or rigid. The ideal fluid waveguide of the perfectly free seabed has an analytical solution of the following form:²

$$p(r, z) = \frac{2\pi i}{H} \sum_{m=1}^{\infty} \sin(k_{z,m} z_s) \sin(k_{z,m} z) \mathcal{H}_0^{(1)}(k_{r,m} r) \quad (35)$$

$$k_{z,m} = \frac{m\pi}{H}, \quad k_{r,m} = \sqrt{k^2 - k_{z,m}^2}, \quad m = 1, 2, 3, \dots$$

The analytical solution of the sound field of the perfectly rigid seabed is the same as that of Eq. (35), except that the vertical wavenumber becomes

$$k_{z,m} = \left(m - \frac{1}{2}\right) \frac{\pi}{H}, \quad m = 1, 2, 3, \dots \quad (36)$$

In this example, the frequency of the sound source is $f = 20$ Hz, and we set the sea depth $H = 100$ m, $z_s = 36$ m, density $\rho = 1$ g/cm³, speed of sound $c = 1500$ m/s, and maximum horizontal range $r_{\max} = 3000$ m. The number of discrete points in the wavenumber domain is set as $M = 2048$, the integral interval is $[0, 2k_0]$ (k_0 is the wavenumber in water), and the spectral truncation order is $N = 10$.

Figures 2(a) and 2(b) depict the wavenumber spectrum of an ideal fluid waveguide with a perfectly free seabed calculated with WISpec. Two peaks (corresponding to propagating modes) appear at $k = 0.077\,678$ and $0.055\,414$ m⁻¹. The presence of these peaks in the wavenumber spectrum indicates that modes are excited by the source. The analytical solution of the discrete spectrum of the ideal fluid waveguide is listed in Table I, with the wavenumbers at the peaks agreeing

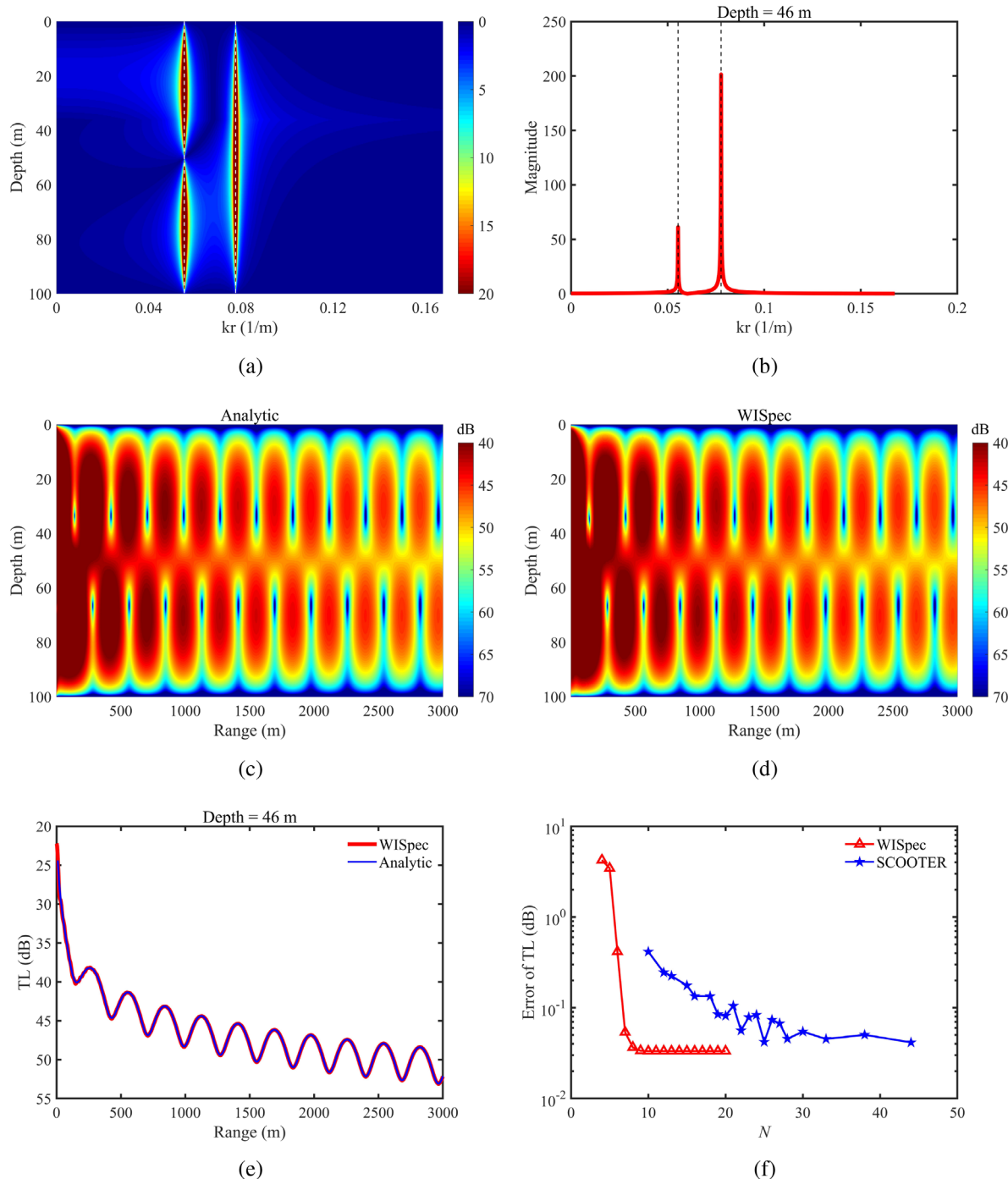


FIG. 2. Wavenumber spectrum of the ideal fluid waveguide with a perfectly free bottom calculated with WI Spec (a); wavenumber spectrum at a depth of $z = 46$ m (b); sound fields calculated with the analytical solution (c) and WI Spec (d); TLs in the r -direction at a depth of $z = 46$ m (e); and the variation trends with N (f).

closely with the analytical solution. The number of discrete points in the wavenumber domain at this stage is only 2048; the accuracy of the wavenumber peaks can be further improved by increasing the number of discrete points in the domain. Figures 2(c)–2(e) show the

pseudocolor and line graphs of the sound fields calculated based on the analytical solution and WI Spec, respectively. The sound fields calculated with WI Spec agree well with those determined with the analytical solution. Figure 2(f) displays the variation in error in the TL fields

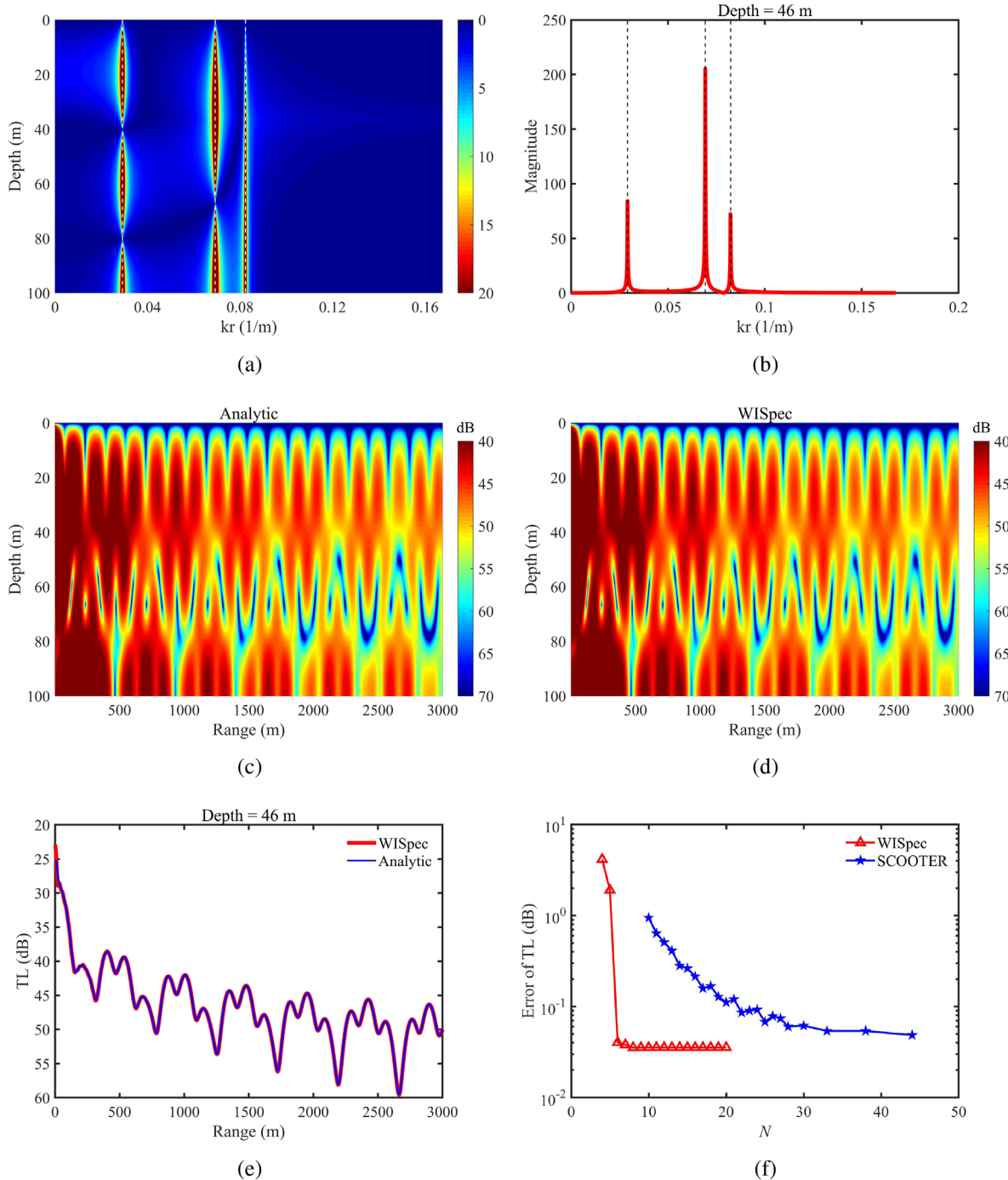


FIG. 3. Wavenumber spectrum of the ideal fluid waveguide with a perfectly rigid bottom calculated with WISpec (a); wavenumber spectrum at a depth of $z = 46$ m (b); sound fields calculated with the analytical solution (c) and WISpec (d); TLs in the r -direction at a depth of $z = 46$ m (e); and the variation trend of the error in the TL field with N (f).

calculated with WISpec and SCOOTER with respect to N . Here, N is the spectral truncation order in WISpec and the number of piecewise linear elements in SCOOTER. To demonstrate the accuracy of the spectral method in solving the depth-separated wave equation, the

same wavenumber integration parameters are used in both WISpec and SCOOTER. The error in the numerical sound fields mainly stems from the error in the Green function. The numerical sound fields are given as a discrete grid comprising 3000 horizontal and 401 vertical

TABLE I. Discrete modes of ideal fluid waveguides (unit: m⁻¹).

Mode order	Free seabed		Rigid seabed	
	Analytic	WISpec	Analytic	WISpec
1	0.077 662	0.077 678	0.082 290	0.082 343
2	0.055 412	0.055 414	0.069 266	0.069 247
3	0.029 153	0.029 139

points spanning 1–3000 and 0–100 m, respectively, with the numerical error calculated as follows:

$$\text{TL}_{\text{error}} = \frac{\sum_{i=1}^{nz} \sum_{j=1}^{nr} |\text{TL}_{i,j} - \overline{\text{TL}}_{i,j}|}{nz \times nr}. \quad (37)$$

Here, nz and nr represent the numbers of discrete points in the vertical and horizontal directions, respectively, and $\overline{\text{TL}}_{i,j}$ denotes the analytical solution for the TL at (z_i, r_j) . Figure 2(f) clearly illustrates that as N increases, the error in the sound field rapidly converges to a very low level and stabilizes. This confirms that the spectral method retains the advantageous property of exponential convergence when solving depth-separated wave equations. In contrast, the error associated with SCOOTER oscillates and decreases linearly, and WISpec exhibits fast convergence, further highlighting the efficiency of the spectral method.

Similarly, Figs. 3(a) and 3(b) display the wavenumber spectrum of an ideal fluid waveguide with a perfectly rigid seabed calculated with WISpec, wherein three peaks appear at $k = 0.082\ 343$, $0.069\ 247$, and $0.029\ 139\ \text{m}^{-1}$. This finding agrees well with the analytical solution presented in Table I, and the sound fields depicted in Figs. 3(c)–3(f) support the same conclusion as the results in Fig. 2, namely, that WISpec can be used to accurately compute the sound field.

B. Analytical example: Pseudolinear-speed waveguide

A pseudolinear-speed waveguide is a waveguide with a sound speed profile that has the following form:²

$$c(z) = \sqrt{\frac{1}{az + b}}. \quad (38)$$

TABLE II. Discrete modes of the pseudolinear-speed waveguide (unit: m⁻¹).

Mode order	Analytical solution	WISpec ($N=15$)	SCOOTER ($N=15$)
1	0.2130	0.2130	0.2131
2	0.2044	0.2045	0.2044
3	0.1943	0.1943	0.1944
4	0.1785	0.1785	0.1785
5	0.1549	0.1549	0.1547
6	0.1188	0.1188	0.1189
7	0.0477	0.0478	0.0478

A pseudolinear-speed waveguide has an analytical solution involving Airy functions [$Ai(\cdot)$ and $Bi(\cdot)$] and their first derivatives [$Ai'(\cdot)$ and $Bi'(\cdot)$], and the horizontal wavenumbers k_r are the roots of a transcendental equation.⁴⁵ In the present example, we assume that the seabed is perfectly rigid, with a sea depth of $H = 100$ m, $a = 5.94 \times 10^{-10}\ \text{s}^2/\text{m}^3$, and $b = 4.16 \times 10^{-7}\ \text{s}^2/\text{m}^3$. The sound source frequency is $f = 50$ Hz, and $M = 4096$; additionally, we use a spectral truncation order of $N = 15$ in WISpec. Table II gives the discrete modes calculated using the three methods. The results obtained with WISpec [shown in Figs. 4(a) and 4(b)] agree well with the analytical solution. The agreement of the sound fields depicted in Figs. 4(c)–4(e) further demonstrates the reliability of WISpec. Figure 4(f) illustrates the variation trends of the errors in the WISpec and SCOOTER models for calculating the sound field as a function of the spectral truncation order or the number of grid points. The figure shows that WISpec achieves faster convergence and yields a lower error than SCOOTER. The same conclusion can be reached for a pseudolinear-speed waveguide with a free bottom, which we do not include here.

C. Pekeris waveguide

The Pekeris waveguide is a classic waveguide in ocean acoustics that consists of a layer of homogeneous water and an acoustic half-space below. In this example, we use the same configuration as that for the ideal fluid waveguide, but the sound source frequency is $f = 50$ Hz, the density in the acoustic half-space is $\rho_\infty = 1.5\ \text{g/cm}^3$, the speed of sound is $c_\infty = 2000\ \text{m/s}$, and the attenuation is $\alpha_\infty = 0.5\ \text{dB}/\lambda$. The sound fields computed using SCOOTER and OASES¹⁵ are presented in Fig. 5 for reference. The sound fields calculated with the three programs are largely consistent, with satisfactory agreement observed in both the sound fields and the TL-line diagram. This further illustrates the ability of WISpec to simulate waveguides with an acoustic half-space (including a continuous spectrum).

In addition to that for point sources, WISpec is capable of computing the sound field excited by line sources. Thus, the sound source is replaced by a line source in this example, and the resulting sound field is depicted in Fig. 6. The sound fields computed with WISpec, SCOOTER, and OASES remain highly similar. To facilitate comparison with SCOOTER and OASES, we normalize the sound field of the line source in WISpec as $p_0 = i\rho_s \omega^2 \mathcal{H}_0^{(1)}(1)/4$ instead of using Eq. (18).

D. Bucker waveguide

The Bucker waveguide is a benchmark for ocean acoustic propagation models.² As illustrated in Fig. 7(a), the difference in sound speed is minimal, resulting in a small number of propagating modes. However, this environment is characterized by a significant contrast in density at the sediment, causing the generation of many virtual modes near the real wavenumber axis. Therefore, the normal mode model, which ignores the continuous spectrum, is not able to provide accurate results for the TL. Additionally, wavenumber integration models can provide precise numerical predictions for the Bucker waveguide. For this particular experiment, the frequency of the sound source was set as $f = 100$ Hz, with a source

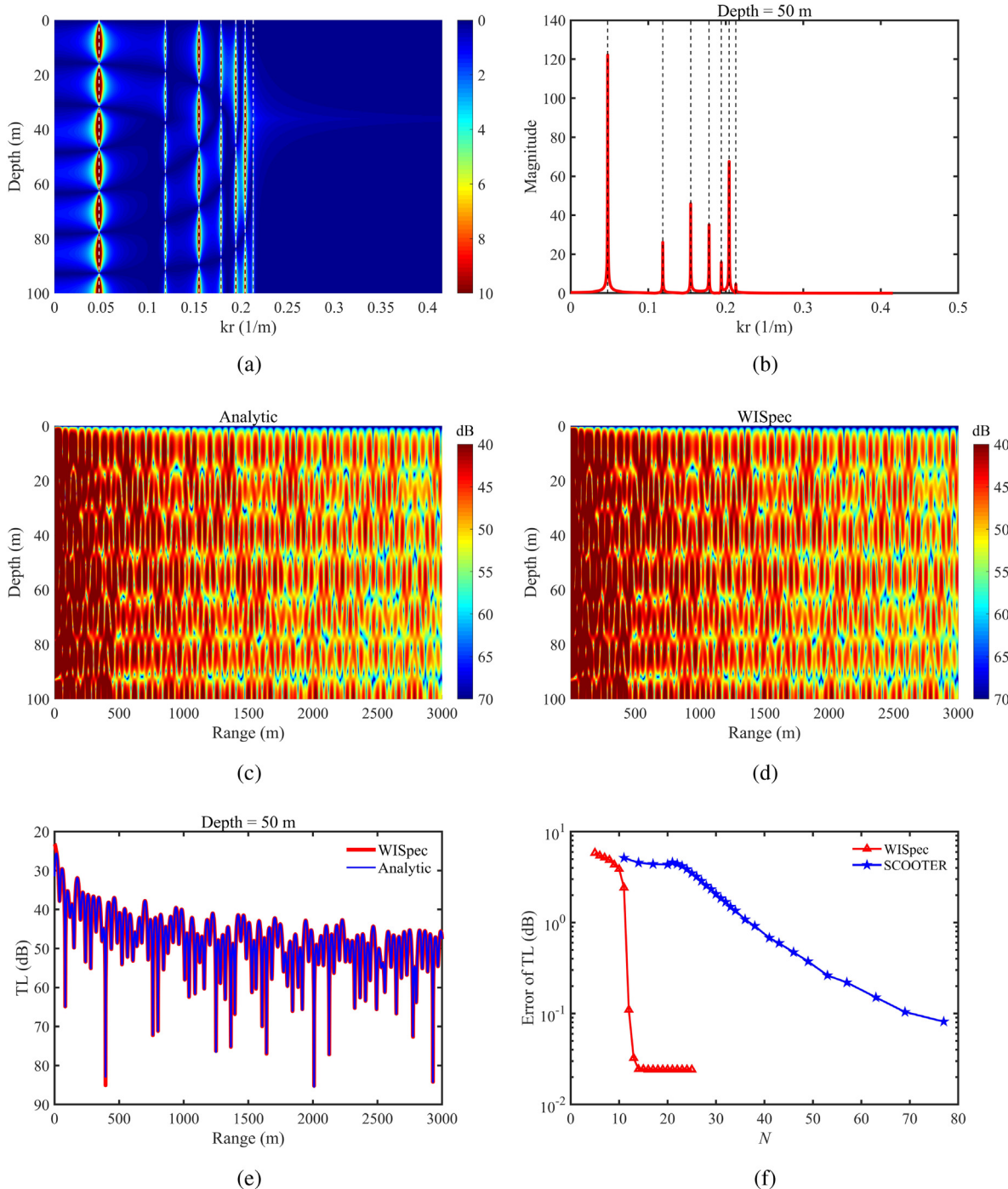


FIG. 4. Wavenumber spectrum of the pseudolinear-speed waveguide with a perfectly rigid bottom calculated with WI Spec (a); wavenumber spectrum at a depth of $z = 50$ m (b); sound fields calculated with the analytical solution (c) and WI Spec (d); TLs in the r -direction at a depth of $z = 50$ m (e); and the variation trend of the error in the TL field with N (f).

depth of $z_s = 30$ m and a sea depth of $H = 240$ m. Additionally, the number of discrete points in the wavenumber domain was $M = 4096$, and the spectral truncation order was $N = 40$, with the integral interval in the range of $[0, 2k_0]$. Figure 8 depicts the sound

fields of the Bucker waveguide calculated using WI Spec, SCOOTER, and OASES. The results produced by the three programs are consistent, except for minor differences noted in the convergence and shadow regions in the near field.

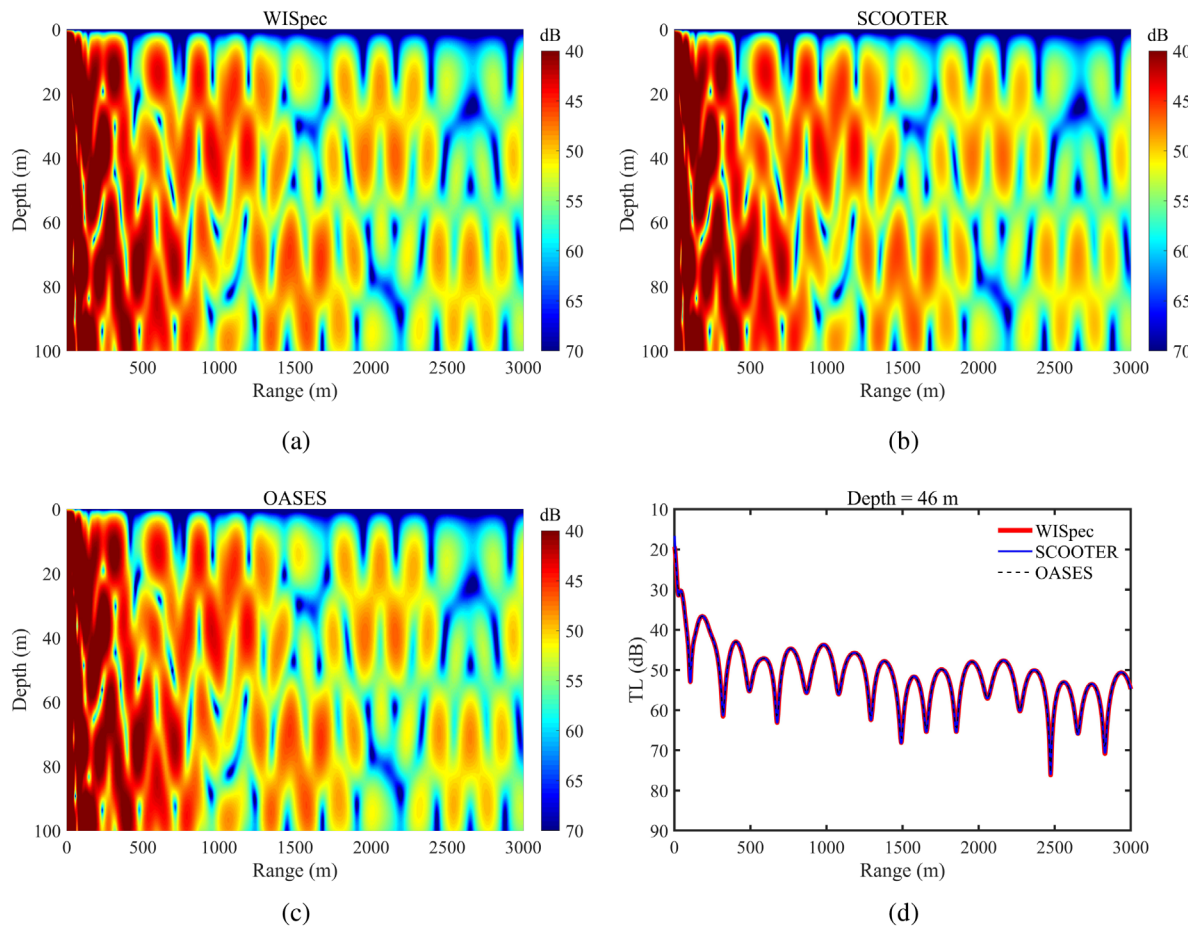


FIG. 5. Sound fields of the Pekeris waveguide calculated with WISpec (a), SCOOTER (b), and OASES (c); TLs in the r -direction at a depth of $z = 46$ m (d).

E. Munk waveguide

The Munk waveguide is a prime example of waveguide with deep-sea acoustic propagation issues. The environment of the ocean consists of layers of seawater with distinct sound speed profiles, such as the Munk profile, and a homogeneous half-space below, as depicted in Fig. 7(b). For this experiment, the frequency of the sound source is set as $f = 50$ Hz, the source depth is $z_s = 100$ m, the sea depth is $H = 5000$ m, and the sound speed profile is²

$$c(z) = 1500.0[1.0 + \varepsilon(\tilde{z} - 1 + \exp(-\tilde{z}))], \quad (39)$$

$$\varepsilon = 0.00737, \quad \tilde{z} = (z - 1300)/650.$$

Moreover, the number of discrete points in the wavenumber domain is $M = 55\,000$, with the integral interval set in the range of $[0, 2k_0]$ and the spectral truncation order set as $N = 400$. Figure 9 displays the sound fields of the Munk waveguide computed with WISpec, SCOOTER, and OASES. The results of the three software programs are remarkably similar, with WISpec and the other two software packages producing TL curves that generally match. However, it should be noted that the results of SCOOTER are

somewhat variable within the range of 10–20 km compared with those of WISpec and OASES.

V. DISCUSSION

To evaluate the computational speed of the algorithm proposed in this paper, we present the time consumption for solving the Green function in the numerical experiments described above, as shown in Table III. The runtimes were obtained by averaging ten tests on the same hardware platform (HUAWEI MateBookX Pro 2018 with an Intel i7-8550U CPU and 8 GB RAM). The times reported in the table were recorded when the simulation results were reliable, and the accuracy was approximately comparable among models. As shown in the table, WISpec exhibits comparable runtime to SCOOTER and OASES for cases with low frequencies and shallow seas and can even achieve slightly faster speeds. However, for deep-sea and high-frequency waveguides, the computational speed of WISpec falls behind that of the two aforementioned mature programs. This highlights the potential for further optimization of WISpec. From the simulation results of the analytical examples, the spectral method achieves higher numerical

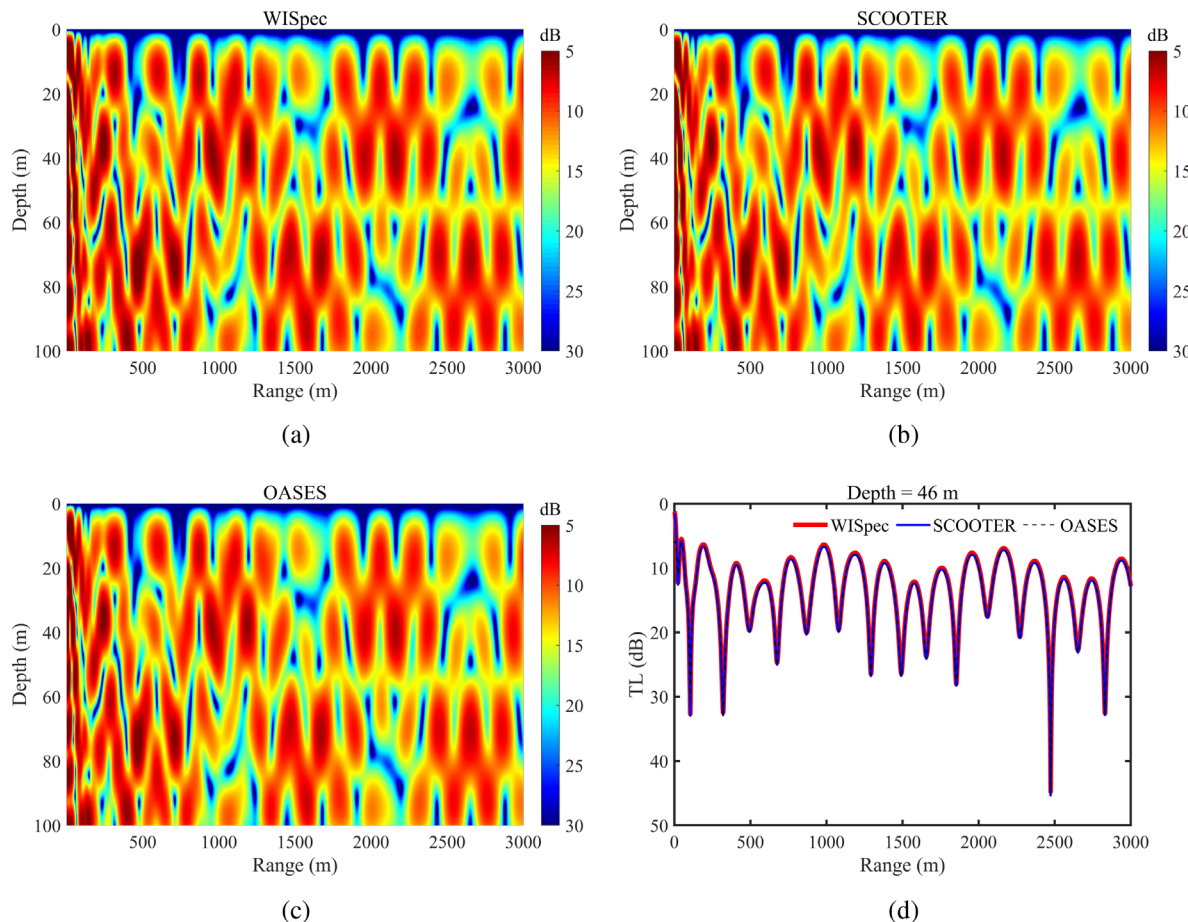


FIG. 6. Sound fields of the Pekeris waveguide of the line source calculated with WISpec (a), SCOOTER (b), and OASES (c); TLs in the x -direction at a depth of $z = 46$ m (d).

accuracy without considering computational time, making it particularly suitable for scenarios that are insensitive to computational complexity, such as the development of benchmark examples.

The aforementioned simulation experiments confirm that WISpec is a robust and accurate program, and the spectral method is effective for solving the depth-separated wave equation. Based on the aforementioned analysis, we can summarize the following features of the proposed algorithm and program.

- With the spectral method applied to solve the depth equation [as depicted in Eq. (29)], there is no need for piecewise linear elements to approximate the environmental parameters. This eliminates the need to subdivide the environment into homogeneous sublayers, avoiding errors resulting from physical discretization in the vertical direction. The error of the spectral algorithm is predominantly associated with the accuracy of spectral approximation; this typically decreases exponentially with increasing truncation order. As such, the spectral algorithm yields accurate and reliable results.
- Discretizing the depth-separated wave equation with the Chebyshev–Tau spectral method yields a block diagonal matrix

[refer to Eq. (33)]. In many cases, the Chebyshev matrix is quasi-diagonally dominant, which enables efficient computations due to its sparsity. Additionally, boundary and interface conditions are incorporated into the global matrix, allowing for a one-time solution for obtaining the Green function of each layer. As a result, the spectral algorithm achieves exceptional numerical stability.

- The spectral method benefits from the exponential decrease in error as the value of N increases. Consequently, WISpec only requires a small truncation order to achieve reliable accuracy, thereby minimizing the size of the discrete matrix. By comparing with existing wavenumber integration models, WISpec exhibits superior computational speed for low-frequency and shallow sea waveguides.
- The finite difference method can only linearly improve accuracy by increasing the number of discrete points after selecting the difference format, and the finite element method is similar. In contrast, spectral algorithms offer an exponential increase in accuracy by increasing the truncation order. This allows for greater precision in scenarios requiring extremely high accuracy and for which the computational cost is a lesser concern. Therefore, spectral algorithms offer clear performance advantages.

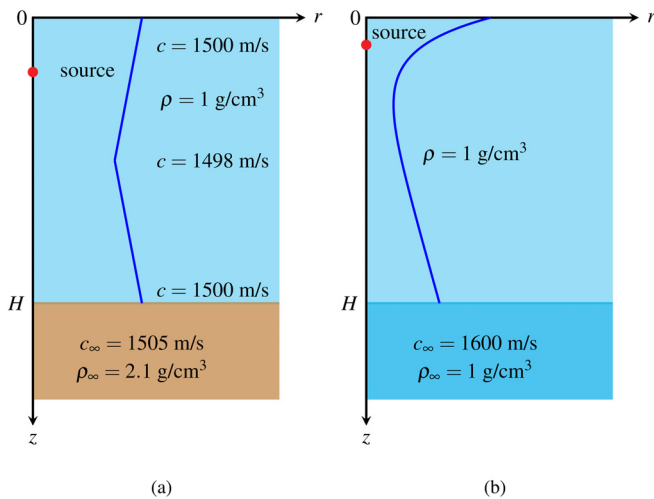


FIG. 7. Schematics of the ocean environment of the Bucker waveguide (a) and Munk waveguide (b).

VI. CONCLUSIONS

This paper proposes a novel approach for solving the depth-separated wave equation of the wavenumber integration model, and the Chebyshev-Tau spectral method is employed to discretize the depth equation and derive a large block diagonal matrix. As additional layers of the medium are incorporated, the discretized block diagonal matrix grows correspondingly, ultimately being transformed into a system of linear equations. These equations can be solved using a variety of methods, yielding spectral coefficients that can then be converted with inverse Chebyshev transforms to obtain depth-dependent Green functions. A complete wavenumber integration model (WISpec) based on this approach is implemented. Initially, the Helmholtz equation is transformed into the wavenumber domain through a Hankel or Fourier transformation. Since horizontally stratified media are considered, the wavenumber kernel function can be represented by the depth-separated wave equation. The algorithm then samples wavenumbers in a predefined interval $[k_{\min}, k_{\max}]$ and solves the Green functions $\Psi(k_r, z)$ in parallel for all the wavenumbers obtained through sampling. After the wavenumber kernel function is obtained, the inverse Hankel or Fourier transform is applied to synthesize the sound-pressure field in the physical space.

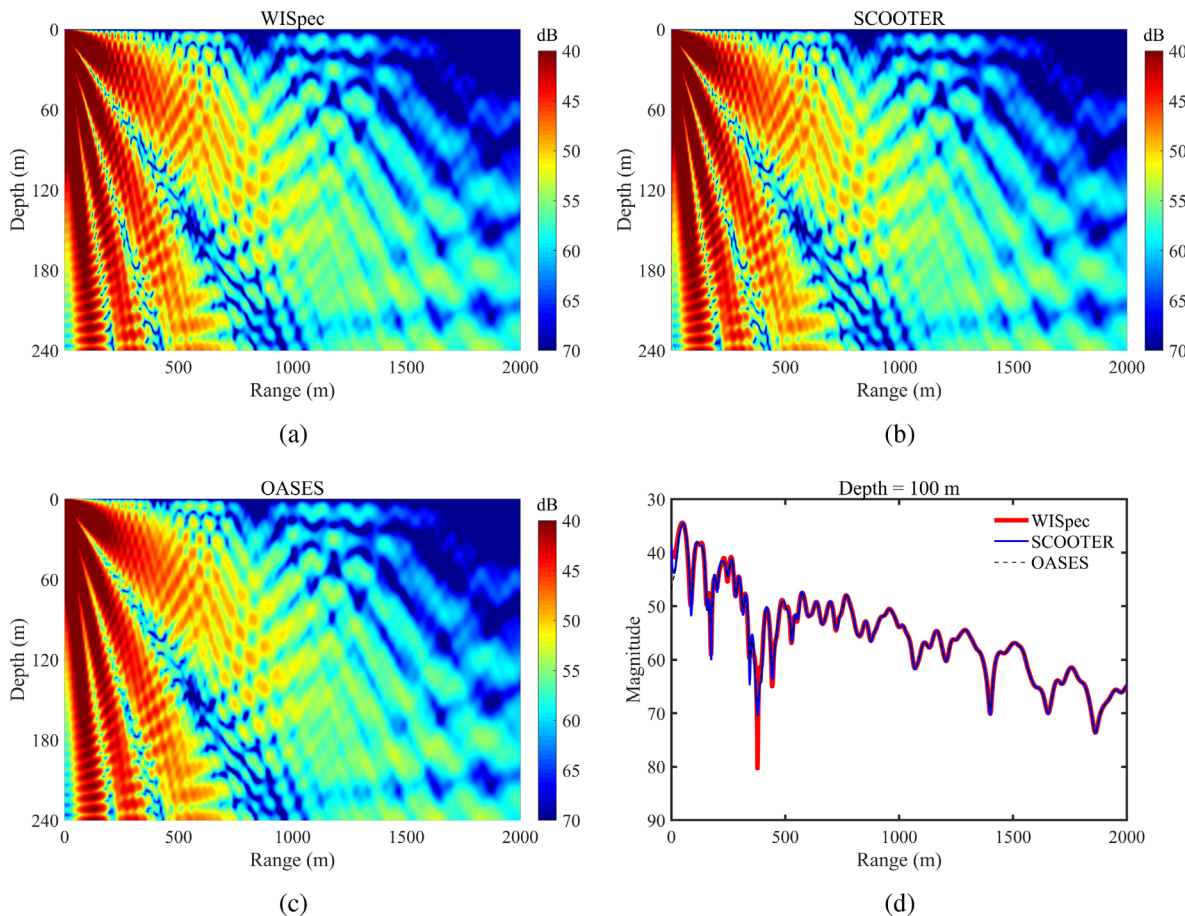


FIG. 8. Sound fields of the Bucker waveguide calculated with WISpec (a), SCOOTER (b), and OASES (c); TLs in the r -direction at a depth of $z = 100 \text{ m}$ (d).

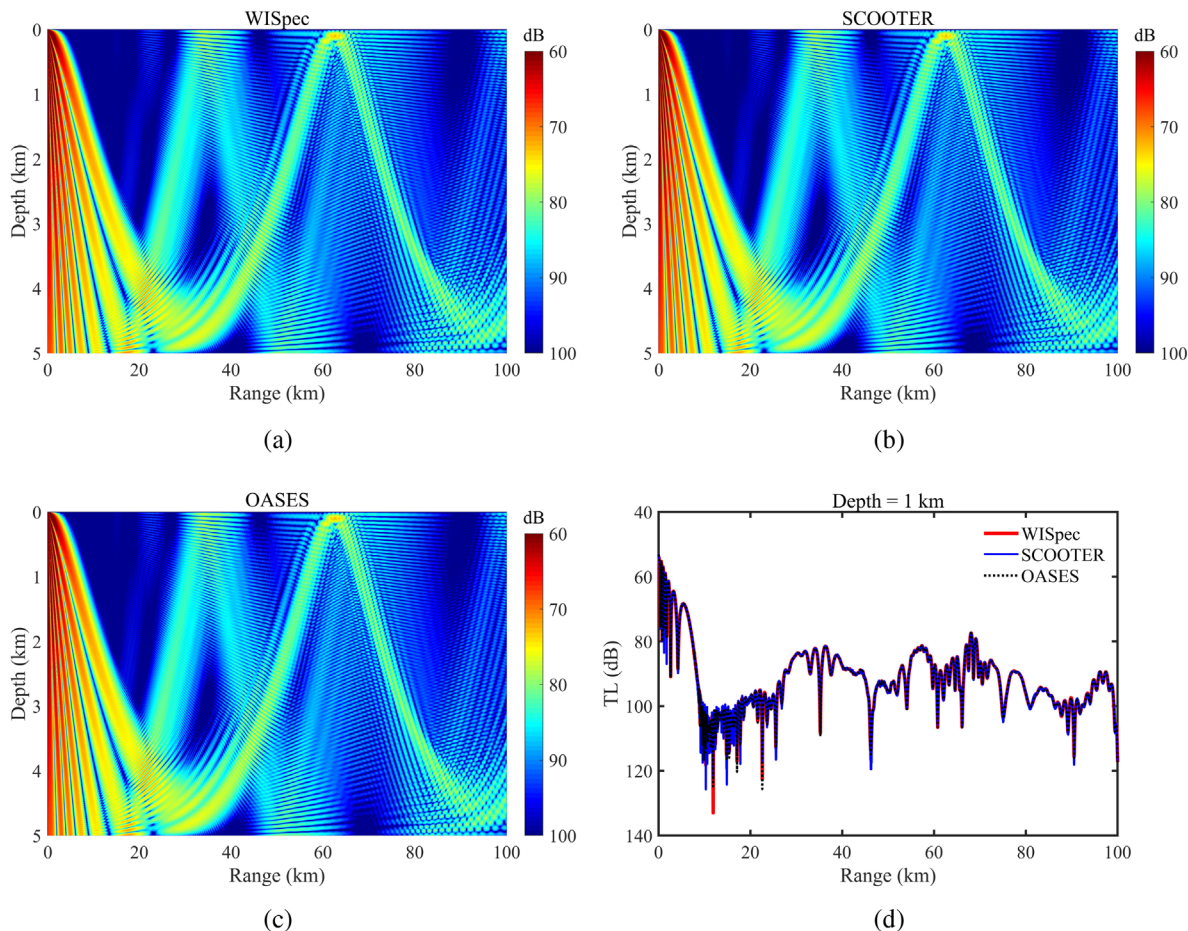


FIG. 9. Sound fields of the Munk waveguide calculated with WISpec (a), SCOOTER (b), and OASES (c); TLs in the r -direction at a depth of $z = 1000$ m (d).

To the best of our knowledge, this algorithm represents the first use of a spectral method for solving the depth-separated wave equation. Spectral methods leverage function approximation and weighted residual discretization to control accuracy. In cases in which ocean

environment parameters exhibit sufficient smoothness, the Green function solution displays exponential convergence. Numerical simulations validate the accuracy and reliability of the new approach and model. Furthermore, our use of the robust and high-precision Chebyshev–Tau spectral method avoids any potential instability in traditional algorithms for solving the depth-separated wave equation.

In terms of its application scope, this model requires that the ocean environment be independent in the r/x direction, which limits the practicality of WISpec to a certain extent. Therefore, there is considerable potential for developing a high-precision wavenumber integration model based on the spectral method for range-dependent waveguides. In addition, elastic sediment models can more accurately simulate the real ocean environment. In the future, WISpec can be further improved to enable the prediction of more complicated ocean acoustic fields.

ACKNOWLEDGMENTS

The authors thank Amlan Datta Chowdhury of the Indian Institute of Technology Madras for his valuable guidance regarding

TABLE III. Runtimes when solving the depth-dependent Green function in the numerical experiments (unit: s).

Case	Special configuration	WISpec	SCOOTER	OASES
Ideal fluid	Free seabed	0.513	0.583	0.694
	Rigid seabed	0.484	0.653	0.703
Pseudolinear	Free seabed	0.814	0.905	1.001
	Rigid seabed	0.845	0.916	0.994
Pekeris	...	0.818	0.899	0.746
	Line source	0.819	0.903	0.726
Bucker	...	1.649	1.164	1.862
Munk	...	155.235	70.882	73.295

the analytical solution of the sound field for the waveguide with a pseudolinear sound speed profile. The authors also thank Zikai Gao of the National University of Defense Technology for his valuable guidance with the installation of OASES.

This work was supported by the National Natural Science Foundation of China under Grant No. 61972406 and by the National Key Research and Development Program of China under Grant No. 2016YFC1401800.

AUTHOR DECLARATIONS

Conflict of Interest

The authors have no conflicts to disclose.

Author Contributions

Houwang Tu: Conceptualization (lead); Data curation (lead); Formal analysis (equal); Investigation (lead); Methodology (equal); Project administration (equal); Software (equal); Validation (lead); Visualization (lead); Writing – original draft (lead); Writing – review & editing (equal). **Yongxian Wang:** Funding acquisition (equal); Project administration (equal); Supervision (equal); Writing – review & editing (equal). **Wei Liu:** Funding acquisition (lead); Writing – review & editing (equal). **Shuqing Ma:** Formal analysis (equal); Visualization (equal). **Xiaodong Wang:** Formal analysis (equal); Visualization (equal).

DATA AVAILABILITY

The data that support the findings of this study are available from the first or corresponding author upon reasonable request.

REFERENCES

- ¹L. M. Brekhovskikh and Y. P. Lysanov, *Fundamentals of Ocean Acoustics* (Springer-Verlag, New York, 2003).
- ²F. B. Jensen, W. A. Kuperman, M. B. Porter, and H. Schmidt, *Computational Ocean Acoustics*, 2nd ed. (Springer, New York, 2011).
- ³P. C. Etter, *Underwater Acoustic Modeling and Simulation* (CRC Press, 2018).
- ⁴C. L. Pekeris, “Theory of propagation of explosive sound in shallow water,” *Geol. Soc. Am. Mem.* **27**, 1–117 (1948).
- ⁵W. M. Ewing, W. S. Jardetzky, and F. Press, *Elastic Wave Inlayered Media* (McGraw-Hill, New York, 1957).
- ⁶W. T. Thomson, “Transmission of elastic waves through a stratified solid medium,” *J. Appl. Phys.* **21**, 89–93 (1950).
- ⁷N. A. Haskell, “The dispersion of surface waves on multilayered media,” *Bull. Seismol. Soc. Am.* **43**, 17–34 (1953).
- ⁸B. Kennett, *Seismic Wave Propagation in Stratified Media* (ANU Press, 2009).
- ⁹B. L. N. Kennett, “Reflections, rays, and reverberations,” *Bull. Seismol. Soc. Am.* **64**, 1685–1696 (1974).
- ¹⁰B. L. N. Kennett and N. J. Kerry, “Seismic waves in a stratified half space,” *Geophys. J. Int.* **57**, 557–583 (1979).
- ¹¹H. Schmidt and F. B. Jensen, “A full wave solution for propagation in multilayered viscoelastic media with application to Gaussian beam reflection at fluid solid interfaces,” *J. Acoust. Soc. Am.* **77**, 813–825 (1985).
- ¹²H. Schmidt and G. Tango, “Efficient global matrix approach to the computation of synthetic seismograms,” *Geophys. J. Int.* **84**, 331–359 (1986).
- ¹³F. B. Jensen, “On the use of stair steps to approximate bathymetry changes in ocean acoustic models,” *J. Acoust. Soc. Am.* **104**, 1310–1315 (1998).
- ¹⁴H. Schmidt, *User’s Guide of SAFARI, Seismo-Acoustic Fast Field Algorithm for Range-Independent Environments* (SACLANT Undersea Research Centre, 1988).
- ¹⁵H. Schmidt, OASES: *User Guide and Reference Manual (Version 3.1)* (Department of Ocean Engineering, Massachusetts Institute of Technology, 2020).
- ¹⁶M. B. Porter, “SCOOTER: A finite element FFP code,” <https://oalib-acoustics.org/models-and-software/acoustics-toolbox/> (2009).
- ¹⁷S. Ivansson, *RPRESS Models For Seismo-Acoustic Wave Fields in Range-Independent Fluid-Solid Media* (Swedish Defence Research Agency, 2022).
- ¹⁸S. Shanbhag, S. Mittal, and Y. M. Joshi, “Spectral method for time-strain separable integral constitutive models in oscillatory shear,” *Phys. Fluids* **33**, 113104 (2021).
- ¹⁹S. A. Orszag, “Comparison of pseudospectral and spectral approximation,” *Stud. Appl. Math.* **51**, 253–259 (1972).
- ²⁰D. Gottlieb and S. A. Orszag, *Numerical Analysis of Spectral Methods* (Society for Industrial and Applied Mathematics, 1977).
- ²¹C. Canuto, M. Y. Hussaini, A. Quarteroni, and T. A. Zang, *Spectral Methods in Fluid Dynamics* (Springer, Berlin/Heidelberg, 1988).
- ²²B. Guo, *Spectral Methods and Their Applications* (World Scientific, 1998).
- ²³J. P. Boyd, *Chebyshev and Fourier Spectral Methods* (Dover, New York, 2001).
- ²⁴C. Canuto, M. Y. Hussaini, A. Quarteroni, and T. A. Zang, *Spectral Methods Fundamentals in Single Domains* (Springer, Berlin/Heidelberg, 2006).
- ²⁵J. Shen, T. Tang, and L.-L. Wang, *Spectral Methods Algorithms, Analysis and Applications* (Springer-Verlag, Berlin, Germany, 2011).
- ²⁶R. Sabatini and P. Cristini, “A multi-domain collocation method for the accurate computation of normal modes in open oceanic and atmospheric waveguides,” *Acta Acust. Acust.* **105**, 464–474 (2019).
- ²⁷Y. Wang, H. Tu, W. Liu, W. Xiao, and Q. Lan, “Two Chebyshev spectral methods for solving normal modes in atmospheric acoustics,” *Entropy* **23**, 705 (2021).
- ²⁸M. Dzieciuch, “Numerical solution of the acoustic wave equation using Chebyshev polynomials with application to global acoustics,” in *Proceedings of OCEANS* (IEEE, 1993).
- ²⁹H. Tu, Y. Wang, W. Liu, X. Ma, W. Xiao, and Q. Lan, “A Chebyshev spectral method for normal mode and parabolic equation models in underwater acoustics,” *Math. Probl. Eng.* **2020**, 7461314.
- ³⁰H. Tu, Y. Wang, Q. Lan, W. Liu, W. Xiao, and S. Ma, “A Chebyshev–Tau spectral method for normal modes of underwater sound propagation with a layered marine environment,” *J. Sound Vib.* **492**, 115784 (2021).
- ³¹H. Tu, Y. Wang, Q. Lan, W. Liu, W. Xiao, and S. Ma, “Applying a Legendre collocation method based on domain decomposition to calculate underwater sound propagation in a horizontally stratified environment,” *J. Sound Vib.* **511**, 116364 (2021).
- ³²H. Tu, “NM-CT: A Chebyshev–Tau spectral method for normal modes of underwater sound propagation with a layered marine environment in Matlab and Fortran,” <https://github.com/tuhouwang/NM-CT> (2020).
- ³³R. B. Evans, “rimLG: A Legendre–Galerkin technique for differential eigenvalue problems with complex and discontinuous coefficients, arising in underwater acoustics,” https://oalib-acoustics.org/website_resources/Modes/rimLG_2016.zip (2016).
- ³⁴H. Tu, “MultiLC: A Legendre collocation method based on domain decomposition to calculate underwater sound propagation in a horizontally stratified environment in Matlab and Fortran,” <https://github.com/tuhouwang/MultiLC> (2021).
- ³⁵H. Tu, Y. Wang, C. Yang, X. Wang, S. Ma, W. Xiao, and W. Liu, “A novel algorithm to solve for an underwater line sourcesound field based on coupled modes and a spectral method,” *J. Comput. Phys.* **468**, 111478 (2022).
- ³⁶H. Tu, Y. Wang, W. Liu, C. Yang, J. Qin, S. Ma, and X. Wang, “Application of a spectral method to simulate quasi-three-dimensional underwater acoustic fields,” *J. Sound Vib.* **545**, 117421 (2023).
- ³⁷H. Tu, Y. Wang, C. Yang, W. Liu, and X. Wang, “A Chebyshev–Tau spectral method for coupled modes of underwater sound propagation in range-dependent ocean environments,” *Phys. Fluids* **35**, 037113 (2023).
- ³⁸H. Tu, Y. Wang, Y. Zhang, H. Liao, and W. Liu, “Parallel numerical simulation of weakly range-dependent ocean acoustic waveguides by adiabatic modes based on a spectral method,” *Phys. Fluids* **35**, 017119 (2023).
- ³⁹H. Tu, Y. Wang, X. Ma, and X. Zhu, “Applying the Chebyshev–Tau spectral method to solve the parabolic equation model of wide-angle rational approximation in ocean acoustics,” *J. Theor. Comput. Acoust.* **30**, 2150013 (2022).
- ⁴⁰H. Tu, “SMPE: Two spectral methods for solving the range-independent parabolic equation model in ocean acoustics,” <https://github.com/tuhouwang/SMPE> (2021).

⁴¹W. Luo, X. Yu, X. Yang, and R. Zhang, "Analytical solution based on the wave-number integration method for the acoustic field in a Pekeris waveguide," *Chin. Phys. B* **25**, 044302 (2016).

⁴²C. Lanczos, "Trigonometric interpolation of empirical and analytical functions," *J. Math. Phys.* **17**, 123–199 (1938).

⁴³J. Shen and T. Tang, *Spectral and High-Order Methods With Applications*, edited by Y. Chen (Science Press, Beijing, 2006).

⁴⁴M. S. Min and D. Gottlieb, "Domain decomposition spectral approximations for an eigenvalue problem with a piecewise constant coefficient," *SIAM J. Numer. Anal.* **43**, 502–520 (2005).

⁴⁵A. D. Chowdhury, C. P. Vendhan, S. K. Bhattacharyya, and S. Mudaliar, "A Rayleigh-Ritz model for the depth eigenproblem of heterogeneous Pekeris waveguides," *Acta Acust. Acust.* **104**, 597–610 (2018).